Viral PB1-F2 and host IFN-γ guide ILC2 and T cell activity during influenza virus infection

Tarani Kanta Barman[a], Victor C. Huber[b], Jesse L. Bonin[a], Danielle Califano[a], Sharon L. Salmon[a], Andrew N. J. McKenzie[c], and Dennis W. Metzger[a,1]

[a]Department of Immunology and Microbial Disease, Albany Medical College, Albany, NY 12208; [b]Division of Basic Biomedical Sciences, University of South Dakota, 414 E Clark St, Vermillion, South Dakota 57069; and [c]Medical Research Council, Laboratory of Molecular Biology, Cambridge CB2 0QH, United Kingdom

Edited by Peter Palese, Microbiology, Icahn School of Medicine at Mount Sinai, New York, NY; received October 8, 2021; accepted January 9, 2022

Functional plasticity of innate lymphoid cells (ILCs) and T cells is regulated by host environmental cues, but the influence of pathogen-derived virulence factors has not been described. We now report the interplay between host interferon (IFN)-γ and viral PB1-F2 virulence protein in regulating the functions of ILC2s and T cells that lead to recovery from influenza virus infection of mice. In the absence of IFN-γ, lung ILC2s from mice challenged with the A/California/04/2009 (CA04) H1N1 virus, containing nonfunctional viral PB1-F2, initiated a robust IL-5 response, which also led to improved tissue integrity and increased survival. Conversely, challenge with Puerto Rico/8/1934 (PR8) H1N1 virus expressing fully functional PB1-F2, suppressed IL-5$^+$ ILC2 responses, and induced a dominant IL-13$^+$ CD8 T cell response, regardless of host IFN-γ expression. IFN-γ–deficient mice had increased survival and improved tissue integrity following challenge with lethal doses of CA04, but not PR8 virus, and increased resistance was dependent on the presence of IFN-γR$^+$ ILC2s. Reverse-engineered influenza viruses differing in functional PB1-F2 activity induced ILC2 and T cell phenotypes similar to the PB1-F2 donor strains, demonstrating the potent role of viral PB1-F2 in host resistance. These results show the ability of a pathogen virulence factor together with host IFN-γ to regulate protective pulmonary immunity during influenza infection.

influenza | ILCs | IFN-γ | T cells | PB1-F2

Innate lymphoid cells (ILCs) and T cells represent critical populations of cells that have diverse roles in inflammation and protection (1, 2). Both cell populations consist of subsets that differ in cytokine expression and function. While T cells are important for viral clearance, they can also exacerbate lung immunopathology (1, 3–5) Among ILC subsets, ILC2s play a critical role in pulmonary immunity, particularly in maintaining the lung barrier surface (6–9). During infection, ILC2s respond to the epithelial cell–derived cytokines IL-25, IL-33, and thymic stromal lymphopoietin, and produce the type 2 cytokine IL-5 (10–12). This, in turn, can lead to increased eosinophil recruitment and airway hyperreactivity (AHR) (8, 13–15). Like T cells, ILC2s can play both beneficial and detrimental roles during viral lung infection (6–8).

It is known that host cytokines can regulate the activity of ILC and T cell subsets. For example, we previously found that interferon (IFN)-γ deficiency results in enhanced ILC2 activity and increased survival from challenge with the 2009 pandemic strain A/California/04/2009 (CA04) influenza A virus (8). However, our current studies have shown no effect of IFN-γ following challenge with the Puerto Rico/8/1934 (PR8) influenza A virus, a strain that is a commonly used model for the highly virulent 1918 pandemic influenza virus. Although both strains are H1N1 influenza A viruses, they have striking differences in expression of functional PB1-F2, a viral proapoptotic protein that is associated with immunopathology and mortality (16). While the PR8 viral strain expresses full-length PB1-F2, the PB1-F2 gene in the CA04 strain is truncated and nonfunctional (16–20). As a result, the PR8 virus exhibits significantly increased virulence compared to the CA04 viral strain. However, the impact of PB1-F2 on the lymphocyte function that is critical for protection during influenza is not known. A better understanding of the role of pathogen virulence factors in regulating immune cell activity during influenza may aid in designing future therapies for human use.

We hypothesized that the PB1-F2 virulence protein can differentially regulate ILC2 and T cell activity in conjunction with host IFN-γ signaling. To test this hypothesis, we have investigated pulmonary immunity in wild-type (WT) and IFN-γ–deficient BALB/c mice infected with PB1-F2 gene reassortant PR8 and CA04 viruses. Our findings demonstrate that viral virulence genes, together with host factors, play critical roles in regulating both ILC2 and T cell responses during influenza, and this, in turn, determines host survival.

Results

IFN-γ Differentially Affects Susceptibility to CA04 and PR8 Virus Infection. We tested susceptibility of IFN-γ$^{+/+}$ and IFN-γ$^{-/-}$ mice to the commonly used PR8 and CA04 H1N1 strains of influenza A virus. Mice were infected intranasally (i. n.) with 1,000 or 2,000 plaque forming units (PFU) of virus; weight loss and survival were then monitored for 20 d (Fig. 1*A*). IFN-γ$^{-/-}$

Significance

The regulation of functional immune cell plasticity is poorly understood. Host environmental cues are critical, but the possible influence of pathogen-derived virulence factors has not been described. We have used reverse-engineered influenza A viruses that differ in PB1-F2 activity to analyze influenza in mice in the presence or absence of host interferon (IFN)-γ. In the absence of functional PB1-F2 and IFN-γ, lung ILC2s initiated robust IL-5 responses following viral challenge, which led to improved tissue integrity and survival. Conversely, functional PB1-F2 suppressed IL-5$^+$ ILC2 responses and induced a dominant IL-13$^+$ CD8 T cell response regardless of host IFN-γ. These findings demonstrate the critical interplay between the viral virulence factors and host cytokines in regulating protective pulmonary immunity during influenza virus infection.

Author contributions: T.K.B., V.C.H., J.L.B., D.C., and D.W.M. designed research; T.K.B., J.L.B., D.C., and S.L.S. performed research; T.K.B., J.L.B., D.C., and D.W.M. analyzed data; V.C.H., S.L.S., A.N.J.M., and D.W.M. contributed new reagents/analytic tools; and T.K.B., V.C.H., and D.W.M. wrote the paper.

The authors declare no competing interest.

This article is a PNAS Direct Submission.

[1]To whom correspondence may be addressed. Email: metzged@amc.edu.

This article contains supporting information online at http://www.pnas.org/lookup/suppl/doi:10.1073/pnas.2118535119/-/DCSupplemental.

Published February 15, 2022.

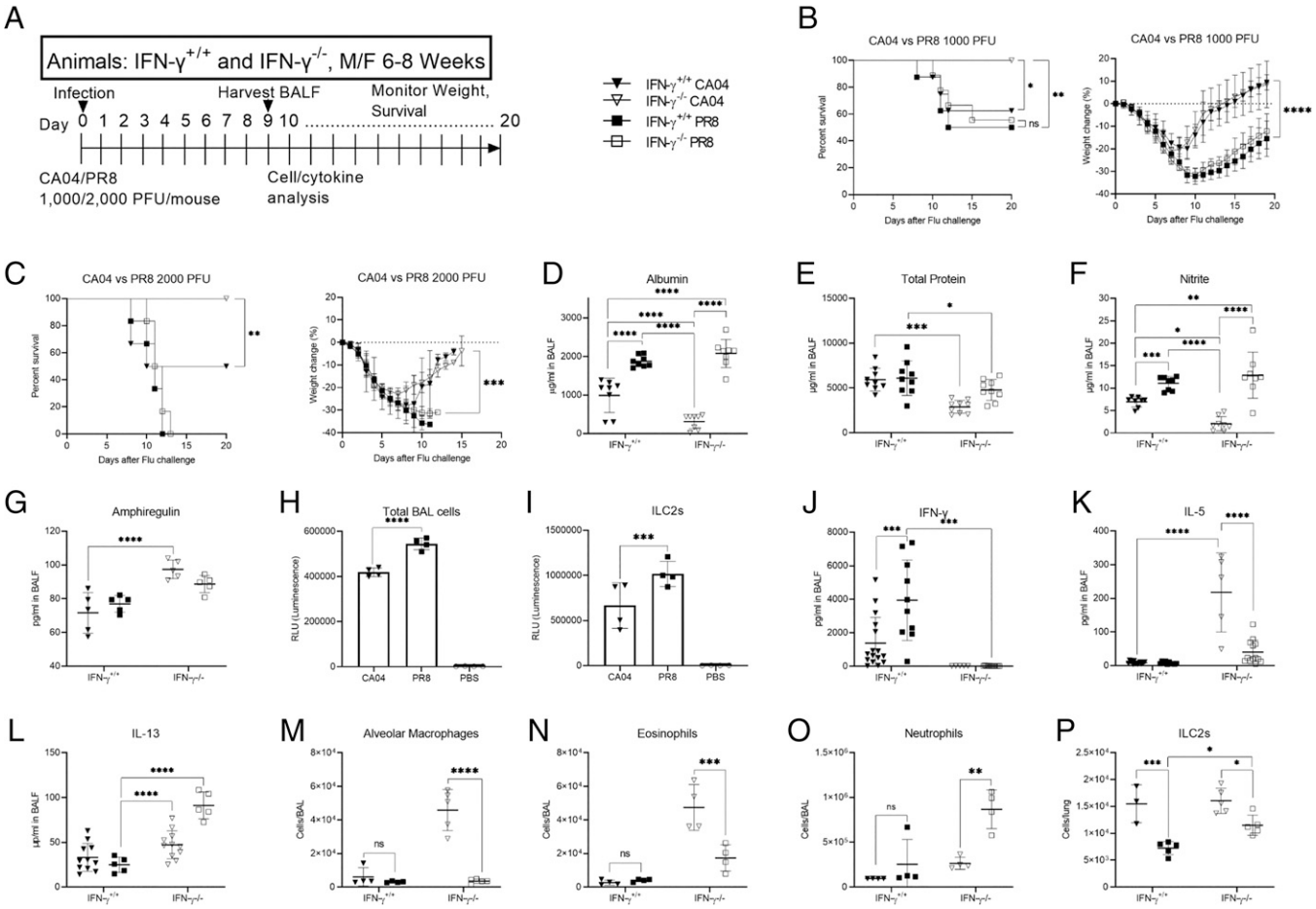

Fig. 1. Survival, tissue pathology, apoptosis, and expression of cell subsets and cytokines of IFN-$\gamma^{+/+}$ and IFN-$\gamma^{-/-}$ BALB/c mice challenged with CA04 or PR8 influenza A virus. (*A*) Protocol for in vivo virus challenge and key to the symbols. Around 6- to 8-wk-old BALB/c mice (6 to 9 mice/group) of either sex were used for all survival studies. (*B*) Survival and weight loss of IFN-$\gamma^{+/+}$ and IFN-$\gamma^{-/-}$ BALB/c mice following challenge with 1,000 PFU/mouse of CA04 or PR8 virus. Mice were monitored daily for 20 d. (*C*) Survival and weight loss of IFN-$\gamma^{+/+}$ and IFN-$\gamma^{-/-}$ BALB/c mice following challenge with 2,000 PFU/mouse of CA04 or PR8 virus. The results are representative of four independent experiments performed in both BALB/c and C57BL/6 mice. Albumin (*D*), total protein (*E*), nitrite (*F*), and amphiregulin (*G*) in Day 9 BALF of mice infected with 2,000 PFU of CA04 or PR8. Each symbol represents an individual mouse, with the solid lines showing means ± SD from 5 to 9 mice/group. Apoptosis in total BAL cells (*H*) and a murine ILC2 cell line (*I*) determined by the Caspase-Glo 3/7 assay. BAL cells were collected in α-minimum essential medium (MEM) containing 1 ng/mL rIL-33 and 10 ng/mL rIL-2 on Day 5 following CA04, PR8, or PBS inoculation. The murine ILC2 cell line was grown for 5 d in the presence of Day 9 BALF collected from CA04- or PR8-infected mice. Data are presented as means ± SD from 4 mice/group. Levels of IFN-γ (*J*), IL-5 (*K*), IL-13 (*L*), alveolar macrophages (*M*), eosinophils (*N*), and neutrophils (*O*) in Day 9 BAL following CA04 or PR8 virus infection. (*P*) ILC2s in Day 9 lung tissue homogenates. Each symbol represents an individual mouse, with the solid lines showing means ± SD from 4 to 14 mice/group. Survival data were analyzed by log-rank Mantel–Cox test, and weight loss data were analyzed by Mann–Whitney *U* test. **P* < 0.05 and ***P* < 0.01. All other statistical analyses were performed by two-way ANOVA. **P* < 0.05; ***P* < 0.01; ****P* < 0.001; and *****P* < 0.0001.

mice were more resistant to CA04 virus infection compared to IFN-$\gamma^{+/+}$ mice, in agreement with our previous findings (8), yet IFN-$\gamma^{+/+}$ and IFN-$\gamma^{-/-}$ mice had no differences in morbidity or mortality following PR8 infection (Fig. 1 *B* and *C*). Initial weight loss was similar between mice infected with CA04 or PR8 virus, confirming virus infection (Fig.1 *B* and *C*), but significant differences were observed beginning on Day 10 postinfection. All IFN-$\gamma^{-/-}$ mice infected with CA04 survived infection with either challenge dose, while IFN-$\gamma^{-/-}$ mice infected with PR8 showed no differences from IFN-$\gamma^{+/+}$ mice challenged with lethal dose $(LD)_{50}$ or LD_{100} of virus (Fig. 1 *B* and *C*). Clinical scoring of disease symptoms indicated significantly greater morbidity following PR8 infection of IFN-$\gamma^{-/-}$ and IFN-$\gamma^{+/+}$ mice compared to CA04 infection. PR8 and CA04 viral burdens and clearance did not differ significantly in the presence or absence of IFN-γ (*SI Appendix*, Fig. S1) despite disparate lethality. This is similar to our previous findings and those of others (8, 21, 22) and suggests that viral load has little impact on ultimate disease outcome.

We further investigated the extent of lung tissue damage after CA04 and PR8 infection by measuring markers such as albumin, total protein, and nitrite. Increased levels of these proteins in bronchoalveolar lavage fluids (BALF) indicate loss of barrier integrity (6, 23). The presence of BALF total protein, albumin, and nitrite following CA04 infection was increased in IFN-$\gamma^{+/+}$ BALB/c mice compared to IFN-$\gamma^{-/-}$ mice (Fig. 1 *D*–*F*). Following PR8 infection, however, there were no significant differences in levels of these markers between IFN-$\gamma^{+/+}$ and IFN-$\gamma^{-/-}$ mice (Fig. 1 *D*–*F*). Similarly, levels of amphiregulin, which help in tissue repair following infection, were greater in IFN-$\gamma^{-/-}$ versus IFN-$\gamma^{+/+}$ BALB/c mice infected with CA04 but did not significantly differ in PR8-infected mice (Fig. 1*G*). These results demonstrated that IFN-γ was detrimental during CA04 infection and caused increased morbidity and mortality because of a reduction in tissue integrity. However, the presence or absence of IFN-γ had little effect in the case of PR8 infection.

Caspase enzymes play an important role in apoptosis (24, 25). The PR8 influenza virus promotes apoptosis of immune

cells, which contributes to immunopathology, but has little influence on viral clearance (26–29). As a measure of apoptosis, we performed a caspase-3/7 assay with total bronchioalveolar lavage (BAL) cells obtained following viral infection (Fig. 1*H*) and with an ILC2 cell line cultured with BALF from animals infected with CA04 or PR8 virus (Fig. 1*I*). The results showed significantly greater caspase activity after PR8 infection compared to CA04 infection. These results agree with earlier work indicating the ability of the PR8 PB1-F2 to promote lethality by enhancing apoptosis and cell death (30, 31).

We next examined cytokine profiles in lungs of IFN-$\gamma^{+/+}$ and IFN-$\gamma^{-/-}$ BALB/c mice infected with CA04 and PR8 virus to determine their potential roles in PR8 lethality versus CA04 resistance. IFN-$\gamma^{+/+}$ and IFN-$\gamma^{-/-}$ animals were infected with 2,000 PFU of virus and Day 9 BALF cytokine profiles were determined. As expected, levels of IFN-γ were significantly greater in IFN-$\gamma^{+/+}$ versus IFN-$\gamma^{-/-}$ mice, and furthermore, IFN-γ levels in PR8-infected IFN-$\gamma^{+/+}$ mice were greater compared to CA04-infected IFN-$\gamma^{+/+}$ mice (Fig. 1*J*). The most striking observation was that IFN-$\gamma^{-/-}$ BALB/c mice displayed a robust IL-5 response after CA04 infection (Fig. 1*K*), whereas IL-13 was the predominant cytokine produced in response to PR8 infection (Fig. 1*L*). There were no significant differences between IFN-$\gamma^{+/+}$ or IFN-$\gamma^{-/-}$ mice in the expression of BALF IL-2, IL-4, IL-9, IL-12, GM-CSF, or TNF-α after infection with CA04 or PR8 virus (*SI Appendix*, Fig. S2). However, compared to IFN-$\gamma^{+/+}$ mice, IFN-$\gamma^{-/-}$ mice did exhibit enhanced IL-10 production following CA04 infection, while PR8 promoted IL-17 production (*SI Appendix*, Fig. S3).

Our results indicated that IFN-$\gamma^{-/-}$ BALB/c mice have reduced tissue damage following CA04 but not PR8 influenza infection compared to IFN-$\gamma^{+/+}$ animals. To characterize the lung cell populations that were expressed following CA04 and PR8 infection and the influence of IFN-γ on cell expression, IFN-$\gamma^{+/+}$ and IFN-$\gamma^{-/-}$ BALB/c mice were infected with 2,000 PFU of CA04 or PR8 virus and levels of alveolar macrophages, eosinophils, and neutrophils in the BAL, and ILC2s in the lung tissues were determined (Fig. 1 *M–P*) using standard gating strategies (*SI Appendix*, Fig. S4 *A–C*). In agreement with earlier reports (32, 33), very few alveolar macrophages were present in IFN-$\gamma^{+/+}$ BALB/c mice following either CA04 or PR8 infection. During CA04 challenge, alveolar macrophage depletion was reversed in the absence of IFN-γ but was still seen following PR8 infection (Fig. 1*M*). Consistent with the increased production of IL-5 in CA04-infected IFN-$\gamma^{-/-}$ mice, numbers of lung eosinophils were greatly elevated compared to PR8-infected mice (Fig. 1*N*). There were only small differences in lung neutrophil counts between WT BALB/c mice infected with CA04 or PR8 virus, although the absence of IFN-γ resulted in greater neutrophil counts in both CA04- and PR8-infected mice (Fig. 1*O*). Of note, IFN-$\gamma^{+/+}$ and IFN-$\gamma^{-/-}$ mice exhibited greater numbers of ILC2s after CA04 infection compared to PR8-infected mice (Fig. 1*P*).

Mortality and Lung Pathology following Challenge with PB1-F2 Reassortant Viruses. The PB1-F2 virulence protein of influenza virus is associated with increased pathogenicity in mice but has little effect on viral burden (16). The PR8 strain expresses full-length PB1-F2, which is also expressed in isolates derived from the 1918 influenza virus, promotes apoptosis of immune cells, and increases animal mortality (26–29). The CA04 virus, on the other hand, possesses a truncated form of the PB1-F2 protein, which is thought to result in reduced pathogenicity (16–18, 20). We thus studied the influence of IFN-γ during infection with reverse-engineered PB1-F2 reassortant viruses (i.e., CA04 containing PR8 PB1-F2, termed CA04 [PR8 PB1-F2] and PR8 containing CA04 PB1-F2, termed PR8 [CA04 PB1-F2]). Each reassortant virus replicated in vivo to the same extent and to the same levels as the parent strains (*SI Appendix*, Figs. S1 and S5). It was again observed that IFN-$\gamma^{-/-}$ mice had increased survival compared to IFN-$\gamma^{+/+}$ mice after challenge with 2,000 PFU of the parent CA04 virus (Fig. 2*A*). However, challenge with the same dose of reassortant CA04 (PR8 PB1-F2) led to 100% lethality regardless of the presence or absence of IFN-γ. Conversely, while no IFN-$\gamma^{+/+}$ or IFN-$\gamma^{-/-}$ mice survived infection with 2,000 PFU of the parent PR8 virus, 40% of WT mice infected with reassortant PR8 (CA04 PB1-F2) virus survived, and this number was further increased to 80% in IFN-$\gamma^{-/-}$ mice (Fig. 2*C*). However, initial body weight loss was essentially identical in all groups, with or without IFN-γ expression (Fig. 2 *B* and *D*), similar to that seen after infection with the parent virus strains (Fig. 1). Further experiments examined weight loss and mortality after challenge with 500, 1,000, or 5,000 PFU of reassortment viruses (*SI Appendix*, Fig. S6). In almost all cases, weight loss was the same among the groups while ultimate survival differed in a manner similar to that seen in Fig. 2. This indicates that although all mice are initially infected to the same degree and show essentially identical, early morbidity, the primary correlate of ultimate survival is likely to be related to the effectiveness of tissue repair and healing.

We next examined lung histopathology after infection with parent CA04 or PR8 virus versus PB1-F2 reassortant viruses. Uninfected, phosphate-buffered saline (PBS)-treated mice maintained the normal architecture of the lung parenchyma, with very few infiltrating cells in the bronchioles and tissue and few differences between IFN-$\gamma^{+/+}$ and IFN-$\gamma^{-/-}$ mice (Fig. 2 E, *i* and *vi*). Only mild–moderate pathology was observed in mice infected with CA04 (Fig. 2 E, *ii*) or reassortant PR8 (CA04 PB1-F2) (Fig. 2 E, *v*) virus, while lesions were severe in IFN-$\gamma^{+/+}$ mice infected with PR8 (Fig. 2 E, *iv*) or reassortant CA04 (PR8 PB1 F2) (Fig. 2 E, *iii*). In IFN-$\gamma^{-/-}$ mice, compared to IFN-$\gamma^{+/+}$ mice, less tissue damage was seen after infection with CA04 (Fig. 2 E, *ii* versus *vii*) or PR8 (CA04 PB1-F2) (Fig. 2 E, *v* versus *x*). Following infection with PR8 or reassortant CA04 (PR8 PB1-F2), however, equivalent and severe pathology was observed in both IFN-$\gamma^{+/+}$ and IFN-$\gamma^{-/-}$ mouse groups (Fig. 2 E, *iii*, *iv*, *viii*, and *ix*). Scoring of the histology sections based on the presence of inflammatory infiltrates, edema, hyperemia and congestion, degeneration of alveolar lining, focal necrosis of alveolar epithelium, and necrotizing bronchitis and bronchiolitis confirmed that all mice infected with PR8 or reassortant CA04 (PR8 PB1-F2) virus had greater degrees of pathology compared to mice infected with CA04 or reassortant PR8 (CA04 PB1-F2) virus (Fig. 2 *F* and *G*). Mucus expression was also examined using the combined periodic acid–Schiff Alcian blue staining technique (Fig. 2 E, *xi–xx*). In response to PR8 and CA04 (PR8 PB1-F2) infection, the lung tissues showed hypersecretion of mucus (Fig. 2 E, *xiii*, *xiv*, *xviii*, and *xix*). Mucin expression was excessive in the lungs of both IFN-$\gamma^{+/+}$ and IFN-$\gamma^{-/-}$ mice after PR8 and CA04 (PR8 PB1-F2) infection compared to mice challenged with CA04 or PR8 (CA04 PB1-F2) (Fig. 2 *H* and *I*). These histology changes correlated with the lethality (Fig. 2 *A–D*) of the individual virus strains.

In the Absence of ILC2s, Host IFN-γ and Viral PB1-F2 Fail to Affect the Course of Influenza. We next determined the role of ILC2s in mediating the effects of host-derived IFN-γ and pathogen-derived PB1-F2 on influenza virus infection. To examine this, we treated ILC2-deficient Rora$^{f/f}$ IL7r^{cre} mice with neutralizing anti–IFN-γ mAb, as in previous studies (8, 34). Rora$^{f/f}$ IL7r^{cre} mice specifically lack ILC2s, while control littermate Rora$^{+/f}$ IL7r^{cre} mice have fully functional ILC2s (34). Our previous studies showed that Rora$^{+/f}$ IL7r^{cre} ILC2-sufficient mice infected with the parent CA04 virus survive significantly better after anti–IFN-γ mAb neutralization compared to animals

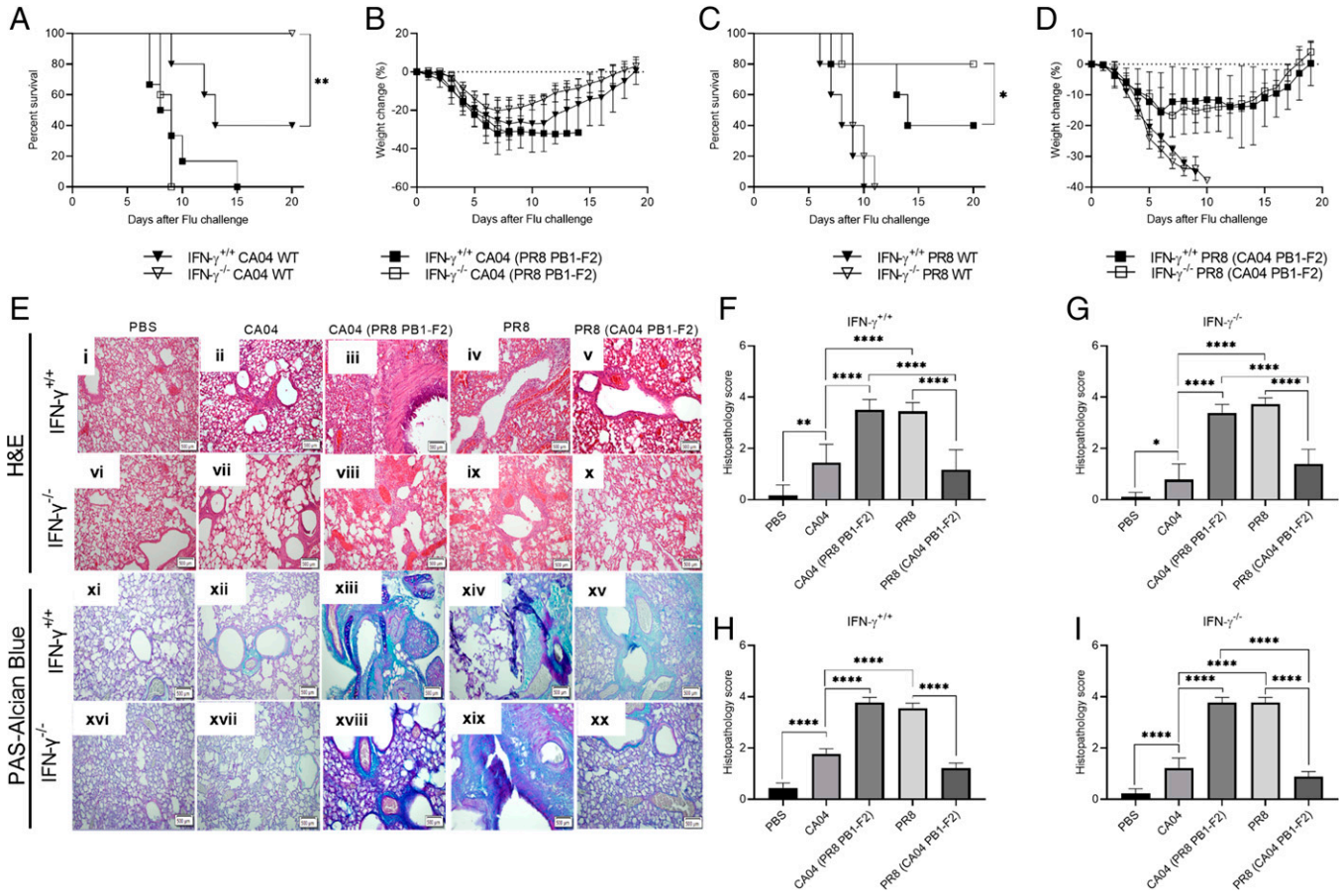

Fig. 2. Mortality and lung pathology following challenge of IFN-$\gamma^{+/+}$ and IFN-$\gamma^{-/-}$ BALB/c mice with CA04 and PR8 PB1-F2 reassortant viruses. Survival (*A*) and weight loss (*B*) following infection of BALB/c IFN-$\gamma^{+/+}$ and IFN-$\gamma^{-/-}$ mice with 2,000 PFU/mouse of CA04 and CA04 (PR8 PB1-F2) virus. Survival (*C*) and weight loss (*D*) following infection of BALB/c IFN-$\gamma^{+/+}$ and IFN-$\gamma^{-/-}$ mice with 2,000 PFU/mouse of PR8 and PR8 (CA04 PB1-F2) virus. Mice were monitored daily for survival for 20 d. A total of 5 to 6 mice/group of either sex were used. The results are representative of two independent experiments and were further confirmed in additional experiments using three different virus challenge doses, as shown in *SI Appendix*, Fig. S6. (*E*) Histopathology of Day 9 lung samples following influenza infection of IFN-$\gamma^{+/+}$ and IFN-$\gamma^{-/-}$ BALB/c mice. Lungs were fixed in 10% formal saline solution, and 5-μm tissue sections were prepared and stained with hematoxylin and eosin (H&E) (*i–x*) or periodic acid–Schiff Alcian blue, pH 2.5 (*xi–xx*), 20× magnification. (Scale Bar, 500 μm.) Control uninfected mice received intranasal PBS on Day 0. (*i*, *vi*, *xi*, and *xvi*) PBS-treated IFN-$\gamma^{+/+}$ and IFN-$\gamma^{-/-}$ mice, (*ii*, *vii*, *xii*, and *xvii*) CA04-infected IFN-$\gamma^{+/+}$ and IFN-$\gamma^{-/-}$ mice, (*iii*, *viii*, *xiii*, and *xviii*) CA04 (PR8 PB1-F2)-infected IFN-$\gamma^{+/+}$ and IFN-$\gamma^{-/-}$ mice, (*iv*, *ix*, *xiv*, and *xix*) PR8-infected IFN-$\gamma^{+/+}$ and IFN-$\gamma^{-/-}$ mice, and (*v*, *x*, *xv*, and *xx*) PR8 (CA04 PB1-F2)-infected IFN-$\gamma^{+/+}$ and IFN-$\gamma^{-/-}$ mice. (*F* and *G*) Histopathology scores from H&E-stained tissue sections based on inflammatory infiltrates, edema, hyperemia, and congestion; degeneration of alveolar lining; focal necrosis of alveolar epithelium; and necrotizing bronchitis and bronchiolitis. (*H* and *I*) Mucus secretion scores from periodic acid–Schiff Alcian blue staining based on intensity of blue staining. Scoring of both H&E and periodic acid–Schiff Alcian blue stained slides are the following: 0 for no changes, 1 for mild changes, 2 for moderate changes, 3 for marked changes, and 4 for severe changes. Statistical analyses were performed by two-way ANOVA. **P* < 0.05; ***P* < 0.01; and *****P* < 0.0001 using 3 to 4 mice/group.

treated with isotype control mAb, while there is no effect of IFN-γ neutralization in ILC2-deficient mice (8). Similarly, after infection with PR8 (CA04 PB1-F2) virus, Rora$^{+/f}$ Il7r^{cre} mice, which contain functional ILC2s, had somewhat improved survival in the absence of IFN-γ (Fig. 3*A*). However, Rora$^{f/f}$ Il7r^{cre} mice, which lack ILC2s, all succumbed to infection regardless of whether IFN-γ was present or absent. In response to infection with CA04 (PR8 PB1-F2), nearly all Rora$^{+/f}$ Il7r^{cre} and Rora$^{f/f}$ Il7r^{cre} mice succumbed to infection regardless of whether ILC2s or IFN-γ were present (Fig. 3*B*). Notably, in all cases and regardless of the reassortant virus used for challenge, ILC2-deficient mice exhibited increased mortality, irrespective of IFN-γ neutralization.

These effects were mirrored by measuring inflammation and tissue damage. Following infection with PR8 (CA04 PB1-F2) virus, nitrite levels in lung tissue were greater in ILC2-deficient versus ILC2-sufficient mice, indicating increased inflammation in the absence of ILC2s (Fig. 3*C*). With CA04 (PR8 PB1-F2) infection, high levels of nitrite were observed, with no significant differences between Rora$^{f/f}$ Il7r^{cre} and Rora$^{+/f}$ Il7r^{cre} mice (Fig. 3*D*). Histopathology analysis showed that the reassortant PR8 (CA04 PB1-F2) virus induced greater inflammation in ILC2-deficient Rora$^{f/f}$ Il7r^{cre} mice compared to Rora$^{+/f}$ Il7r^{cre} mice regardless of anti–IFN-γ mAb treatment (Fig. 3 E, *i–iv*), whereas CA04 (PR8 PB1-F2) infection resulted in severe lesions in both Rora$^{f/f}$ Il7r^{cre} and Rora$^{+/f}$ Il7r^{cre} mice (Fig. 3 E, *v–viii*). Scoring of multiple tissue sections showed lower levels of inflammation in the presence of ILC2s after PR8 (CA04 PB1-F2) virus infection, irrespective of IFN-γ neutralization (Fig. 3*F*). Following CA04 (PR8 PB1-F2) infection, there were no significant differences in histology scores between Rora$^{f/f}$ Il7r^{cre} and Rora$^{+/f}$ Il7r^{cre} mice (Fig. 3*G*). In response to PR8 (CA04 PB1-F2), IL-5 production was greater in ILC2-sufficient mice compared to ILC2-deficient mice (*SI Appendix*, Fig. S7). Taken together, the results indicate that the influenza PB1-F2 virulence factor influences disease susceptibility through its effects on ILC2 activity.

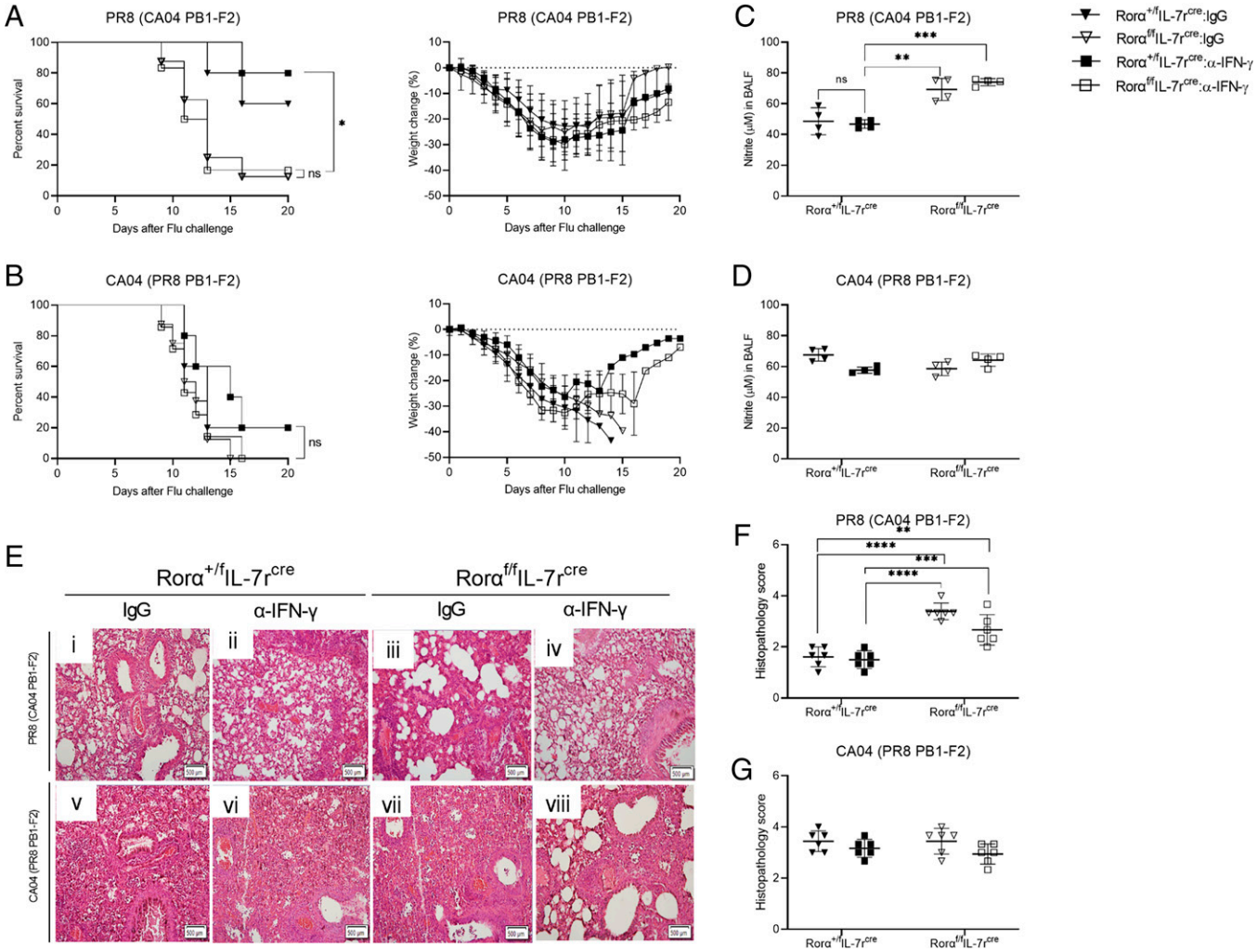

Fig. 3. Failure of ILC2-deficient mice to respond to IFN-γ neutralization during infection with reassortant PR8 (CA04 PB1-F2) or CA04 (PR8 PB1-F2) virus. (*A* and *B*) Survival and weight loss of Rora$^{f/f}$IL-7r^{Cre} and Rora$^{+/f}$IL-7r^{Cre} littermate controls following infection with 500 PFU/mouse of PR8 (CA04 PB1-F2) (*A*) or CA04 (PR8 PB1-F2) (*B*) and treatment with neutralizing anti–IFN-γ mAb or isotype control mAb (5 to 8 mice/group). (*C* and *D*) Levels of nitrite following infection with PR8 (CA04 PB1-F2) (*C*) or CA04 (PR8 PB1-F2) (*D*) virus in Rora$^{+/f}$IL-7r^{Cre} and Rora$^{f/f}$IL-7r^{Cre} littermate control mice (4 mice/group). (*E*, *i–iv*) Representative hematoxylin and eosin (H&E)-stained histopathology tissue sections of Rora$^{+/f}$IL-7r^{Cre} (*i* and *ii*) and Rora$^{f/f}$IL-7r^{Cre} (*iii* and *iv*) mice infected with PR8 (CA04 PB1-F2) virus and treated with anti–IFN-γ (*ii* and *iv*) or isotype control mAb (*i* and *iii*). (*E*, *v–viii*) Representative H&E-stained histopathology tissue sections of Rora$^{+/f}$IL-7r^{Cre} (*v* and *vi*) and Rora$^{f/f}$IL-7r^{Cre} (*vii* and *viii*) mice infected with CA04 (PR8 PB1-F2) virus and treated with anti–IFN-γ (*vi* and *viii*) or isotype control mAb (*v* and *vii*). (*F* and *G*). Histology scores from 4 mice/group at 20× magnification. (Scale Bar, 500 μm.) For neutralization of IFN-γ, ILC2-deficient and sufficient mice were injected intraperitoneal (i.p). with 600 μg anti–IFN-γ mAb (clone XMG1.2; BioXcell) or IgG isotype control on Days 2, 4, 6, 7, 8, 10, 11, and 12 postinfection. Statistical analyses were performed by two-way ANOVA. *$P < 0.05$; **$P < 0.01$; ***$P < 0.001$; ****$P < 0.0001$; and ns, not significant.

Differential ILC2 Activation in Response to CA04 and PR8 PB1-F2 Virulence Factor. Since ILC2s are essential for protection at pulmonary barrier surfaces (6, 7) and can express IL-5 (13–15), we quantified numbers of IL-5+ ILC2s after influenza infection (*SI Appendix*, Fig. S8). Nearly all cells expressing IL-5 after CA04 influenza infection were lineage negative and CD127^{+} KLRG1^{+} and CD90.2^{+} ILC2s (Fig. 4*A*). At early time points after CA04 infection, there was little production of IL-5 by lung ILC2s, but by Day 9, during the recovery stage of infection, IFN-γ$^{-/-}$ mice exhibited significantly increased numbers of IL-5^{+} ILC2s compared to IFN-γ$^{+/+}$ mice (Fig. 4 *B–E* and *SI Appendix*, Fig. S9). Again, mice infected with CA04 or PR8 (CA04 PB1-F2) virus expressed significantly more ILC2s and IL-5^{+} ILC2s compared to mice challenged with PR8 or CA04 (PR8 PB1-F2) virus (Fig. 4 *D* and *E*). IFN-γ$^{-/-}$ mice also expressed increased levels of amphiregulin and IL-10 after challenge with PR8 (CA04 PB1-F2) compared to IFN-γ$^{+/+}$ mice (*SI Appendix*, Fig. S3). Taken together, our results indicate that activation of ILC2s can improve host survival following CA04 infection in the absence of IFN-γ and that the functional PB1-F2 from PR8 virus can inhibit this ILC2-mediated protection. These findings suggest the concept of a strain-specific contribution of PB1-F2 and ILC2s in protection against influenza virus infection.

Direct IFN-γ Signaling of ILC2s Mediates Greater Susceptibility to Influenza. The above results indicated that the influence of IFN-γ and PB1-F2 on host resistance and mortality required the presence of ILC2s. To understand if these effects were directly mediated by IFN-γ signaling in ILC2s, we utilized IFN-γR1$^{f/f}$ Rorα^{cre} mice, which specifically lack IFN-γ receptors on ILC2s. We found that, compared to littermate IFN-γR1$^{+/f}$ Rorα^{cre} controls, IFN-γR1$^{f/f}$ Rorα^{cre} mice had enhanced survival following CA04 infection but not PR8 infection (Fig. 5 *A* and *B*). This

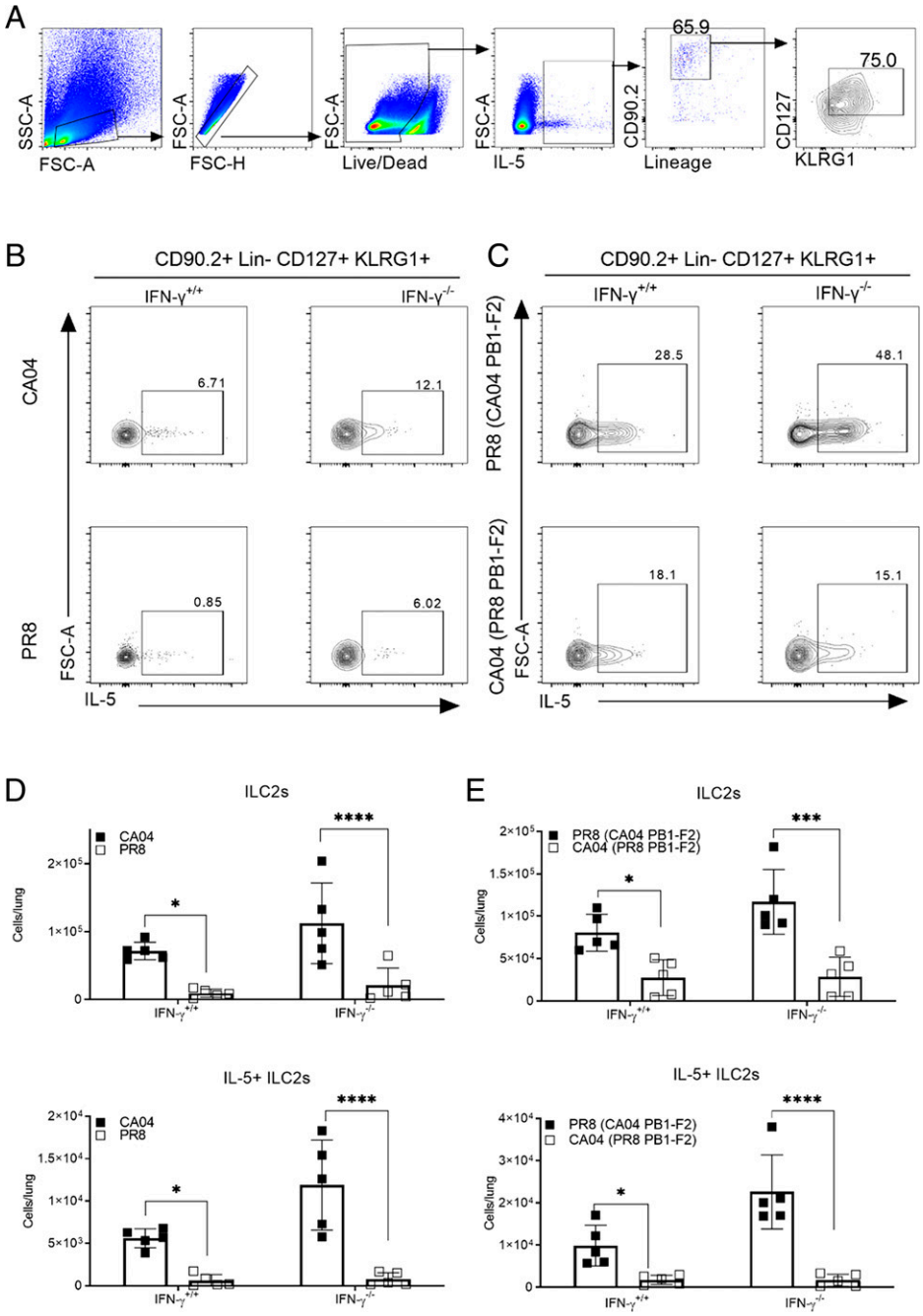

Fig. 4. ILC2 cytokine expression after CA04 or PR8 WT or reassortant virus infection of IFN-$\gamma^{+/+}$ and IFN-$\gamma^{-/-}$ BALB/c mice. Lung cells were harvested 9 d after infection with 50 PFU/mouse and restimulated ex vivo with PMA (50 ng/mL) and ionomycin (500 ng/mL) in the presence of brefeldin A (10 μg/mL). (*A*) Flow cytometry confirmed the identity of IL-5–positive cells as ILC2s. FSC, forward scatter; SSC, side scatter. (*B*) Representative contour plots of IL-5^+ ILC2s following CA04 and PR8 infection. (*C*) IL-5^+ ILC2s following PR8 (CA04 PB1 F2) and CA04 (PR8 PB1 F2) infection. (*D* and *E*) Profiles of total ILC2s and IL-5^+ ILC2s following infection with CA04 or PR8 virus (*D*) and reassortant PR8 (CA04 PB1-F2) or CA04 (PR8 PB1-F2) virus (*E*) in the presence or absence of IFN-γ. The data are presented as means ± SD from 5 mice/group and are representative of two to three independent experiments. Statistical analyses were performed by two-way ANOVA. *$P < 0.05$; ***$P < 0.001$; and ****$P < 0.0001$.

suggests that the increased resistance to CA04 infection that was observed in global, IFN-γ–deficient animals or animals treated with neutralizing anti–IFN-γ mAb was due to an absence of IFN-γ signaling in ILC2s. Thus, as expected, IFN-γR1$^{f/f}$ Rorα^{cre} mice that were infected with CA04 showed lower amounts of edema compared to PR8-infected mice (Fig. 5*C*). Levels of BALF total protein, an indicator of tissue integrity, was also significantly lower in CA04-infected IFN-γR1$^{f/f}$ Rorα^{cre} mice compared to IFN-γR1$^{+/f}$ Rorα^{cre} mice and to infection of either mouse strain with PR8 (Fig. 5*D*). Levels of IL-5 were significantly greater in IFN-γR1$^{f/f}$ Rorα^{cre} mice infected with CA04 infection compared to IFN-γR1$^{+/f}$ Rorα^{cre} littermate controls (Fig. 5*E*), but this effect was not seen in PR8-infected mice. Similarly, the levels of IL-10 (Fig. 5*F*) and amphiregulin (Fig. 5*G*) were greater in IFN-γR1$^{f/f}$ Rorα^{cre} mice infected with CA04 infection compared to IFN-γR1$^{+/f}$ Rorα^{cre} littermate controls. Expression of IL-13, a correlate of lethality, was greater after PR8 infection, regardless of the presence or absence of ILC2

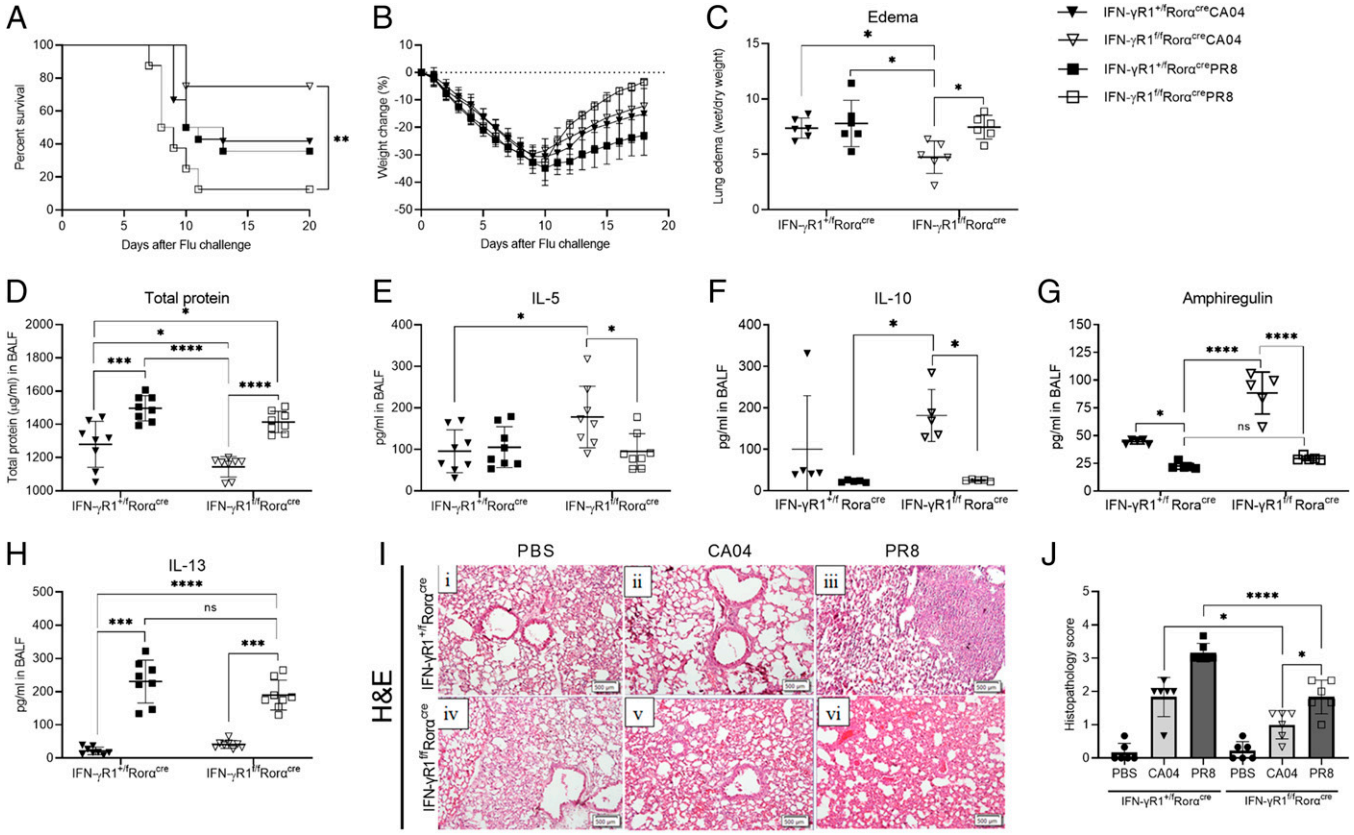

Fig. 5. Viral infection in mice lacking ILC2-specific IFN-γ signaling. Survival (*A*) and weight loss (*B*) in IFN-γR1$^{f/f}$Rorα^{Cre} and IFN-γR1$^{+/f}$Rorα^{Cre} littermate controls following infection with CA04 or PR8 influenza virus. Lung edema (*C*), BALF total protein (*D*), BALF IL-5 (*E*), BALF IL-10 (F), BALF amphiregulin (*G*), and BALF IL-13 (*H*) in IFN-γR1$^{f/f}$Rorα^{Cre} and IFN-γR1$^{+/f}$Rorα^{Cre} littermate control mice on Day 9 after viral infection. Each symbol represents an individual mouse: 5 to 8 mice/group. (*I*) Representative Day 9 hematoxylin and eosin (H&E)-stained lung sections from IFN-γR1$^{+/f}$Rorα^{Cre} (*I*, *i–iii*) and IFN-γR1$^{f/f}$Rorα^{Cre} (*I*, *iv–vi*) mice challenged with PBS (*I*, *i* and *iv*), CA04 virus (*I*, *ii* and *v*), or PR8 virus (*I*, *iii* and *vi*) at 20× magnification. (Scale Bar, 500 μm.) (*J*) H&E histology scores: 4 mice/group. Survival data were combined from two independent experiments (8 to 14 per group) and analyzed by log-rank Mantel–Cox test. All other data are presented as means ± SD, and statistical analyses were performed by ANOVA. *$P < 0.05$; **$P < 0.01$; ***$P < 0.001$; ****$P < 0.0001$; and ns, not significant.

IFN-γ signaling (Fig. 5*H*). IFN-γR1$^{+/f}$ Rorα^{cre} littermates infected with CA04 virus showed minimal lung pathology while there was severe inflammation and tissue damage following PR8 virus, compared to PBS-treated, uninfected control mice (Fig. 5 I, *i–iii*). Lesions were relatively mild in all IFN-γR1$^{f/f}$ Rorα^{cre} mice infected with CA04 or PR8 virus (Fig. 5 I, *v* and *vi*). Histopathology scoring confirmed the decreases in lung pathology observed in the absence in ILC2 IFN-γ signaling (Fig. 5*J*).

IL-13 Is Detrimental during PR8 Influenza Virus Infection. In our previous work, we found that IL-5 played a protective role in CA04 virus infection (8). However, IL-13 expression was preferentially increased in PR8 infection and associated with exacerbated pathogenesis. Thus, we examined the role of IL-13 after infection with PR8 or reassortant CA04 (PR8 PB1-F2) virus using IL-4$^{-/-}$ IL-13$^{-/-}$–deficient mice. Both IL-4 and IL-13 exert their functions through different combinations of shared receptor chains (35) and could have redundant activity, an issue that we avoided using double-deficient animals. BALB/c knockout and WT control mice were infected with 1,000 PFU and observed for morbidity and mortality (Fig. 6 *A–D*). Compared to IL-4$^{+/+}$ IL-13$^{+/+}$ controls, IL-4$^{-/-}$ IL-13$^{-/-}$ mice showed relatively more resistance to PR8 (Fig. 6*A*) and CA04 (PR8 PB1-F2) virus infection (Fig. 6*C*). However, IL-4$^{+/+}$ IL-13$^{+/+}$ and IL-4$^{-/-}$ IL-13$^{-/-}$ mice showed no significant differences in mortality and morbidity in response to infection with CA04 and PR8 (CA04 PB1-F2) (*SI Appendix*, Fig. S10). IL-13 is known to induce excessive mucus production and airway obstruction in response to influenza infection. Lung tissue sections stained with periodic acid–Schiff Alcian blue demonstrated significantly greater levels of mucin secretion in IL-4$^{+/+}$ IL-13$^{+/+}$ mice in response to PR8 and reassortant CA04 (PR8 PB1-F2) virus infection compared to IL-4$^{-/-}$ IL-13$^{-/-}$ mice (Fig. 6 *E* and *F*). Histological changes were found to be greater in IL-4$^{+/+}$ IL-13$^{+/+}$ mice than in IL-4$^{-/-}$ IL-13$^{-/-}$ mice in response to PR8 and CA04 (PR8 PB1-F2) virus (Fig. 6 *G* and *H*). Consistent with the histology analyses, edema as assessed by differences in wet/dry weight was similarly greater in IL-4$^{+/+}$ IL-13$^{+/+}$ mice than in IL-4$^{-/-}$ IL-13$^{-/-}$ mice (Fig. 6*I*). Granzyme B, which is an important marker for tissue pathology, was also found at greater levels in the BALF of IL-4$^{+/+}$ IL-13$^{+/+}$ mice compared to IL-4$^{-/-}$ IL-13$^{-/-}$ mice (Fig. 6*J*).

IL-13 Production during PR8 Influenza Virus Infection Derives from CD8 T Cells. Several cellular sources of IL-13, such as ILC2s, T cells, and natural killer (NK) cells, have been described (36). In our studies, high levels of IL-13 were observed in response to PR8 but not CA04 infection (Fig. 1*L*). The majority of IL-13–producing cells following PR8 challenge were found to be CD3$^+$ T cells, with a small population of CD3$^+$ CD335$^+$ NK cells also expressing IL-13 (Fig. 7*A*). However, few IL-13$^+$ ILC2s or other cells could be detected. Nearly all IL-13$^+$ T cells were CD8 T cells with only some CD4 T cells producing this

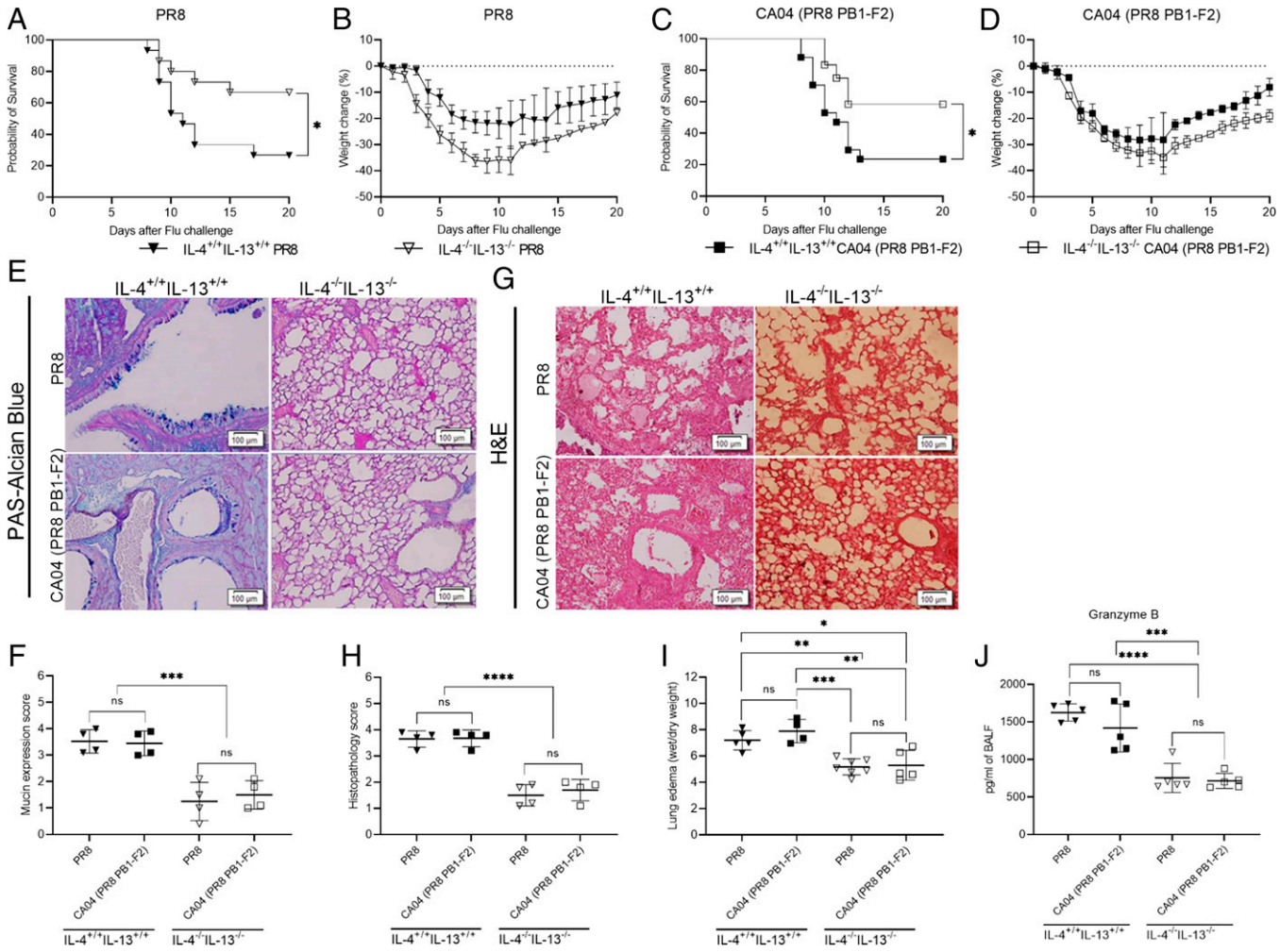

Fig. 6. Lethality and pathogenicity of PR8 and CA04 (PR8 PB1-F2) influenza viruses in BALB/c IL-$4^{+/+}$IL-$13^{+/+}$ and IL-$4^{-/-}$IL-$13^{-/-}$ mice. Survival (*A*) and weight loss (*B*) following infection with PR8 and survival (*C*) and weight loss (*D*) following infection with CA04 (PR8 PB1-F2) in BALB/c IL-$4^{+/+}$IL-$13^{+/+}$ and IL-$4^{-/-}$IL-$13^{-/-}$ mice. The results were pooled from two independent experiments (12 to 17 mice/group). (*E* and *F*) Representative periodic acid–Schiff Alcian blue staining and scoring of Day 9 lung sections following infection with PR8 or CA04 (PR8 PB1-F2) virus. (*G* and *H*) Representative lung tissue hematoxylin and eosin (H&E) staining and scoring at 20× magnification. (Scale Bar, 100 μm [4 mice/group]). (*I*) Lung edema determined by wet/dry weight ratios (5 to 7 mice/group). (*J*) BALF granzyme B levels (5 mice/group). Survival data were combined from two independent experiments analyzed by the log-rank Mantel–Cox test. For *F*, *G*, and *I*, each symbol represents an individual mouse, and the data are presented as means ± SD. Statistical analyses were performed by two-way ANOVA. $*P < 0.05$; $**P < 0.01$; $***P < 0.001$; $****P < 0.0001$; and ns, not significant.

cytokine after PR8 infection (Fig. 7 *B–E*). No significant differences were observed in IL-13 T cell levels between IFN-$\gamma^{+/+}$ and IFN-$\gamma^{-/-}$ mice (Fig. 7 *B–E*), which is consistent with our survival results in PR8-challenged mice (Fig. 1 *B* and *C*). We conclude that the detrimental effects of IL-13 during PR8, but not CA04 virus infection, are due to PB1-F2–mediated activation of CD8 T cells; these IL-13^{+} CD8 cells could represent a Tc2 population based on the increased granzyme B expression seen in Fig. 6*J*.

Discussion

We found that neutralization of IFN-γ enhanced protection against the pandemic H1N1 CA04 influenza A virus but did not influence susceptibility to the H1N1 PR8 strain. In the absence of IFN-γ, increased resistance following the CA04 virus challenge correlated with reduced lung inflammation and heightened production of IL-5 by ILC2s. Conversely, following PR8 challenge, we observed greater pathology and increased production of IL-13 by CD8 T cells, which correlated with detrimental mucin production. By exploiting reverse engineering to generate PB1-F2 gene reassortant virus strains, the differential effects of IFN-γ during CA04 and PR8 infection were found to be due to disparate PB1-F2 expression. Specifically, the greatest protection from viral infection was observed in the absence of both functional PB1-F2 and IFN-γ, and this protection was dependent upon lack of IFN-γR signaling in the lung ILC2 cell population. In the presence of these molecules, mice were highly susceptible to infection. This study revealed interconnected roles for influenza virus PB1-F2 and host IFN-γ in regulating the protective and detrimental effects of ILC2s.

Our results established the unique observation that neutralization of IFN-γ can mediate enhanced resistance to H1N1 CA04 influenza infection, while PR8 infection results in significant pathogenesis irrespective of IFN-γ expression. The results further showed that protection against CA04 virus infection correlated with increased IL-5 production and increased tissue integrity, similar to our earlier studies (8), while IL-13 upregulation during PR8 infection was associated with increased mucin expression and lethality. ILC2s were the major producer of IL-5 in the lungs of infected animals, while almost all IL-13

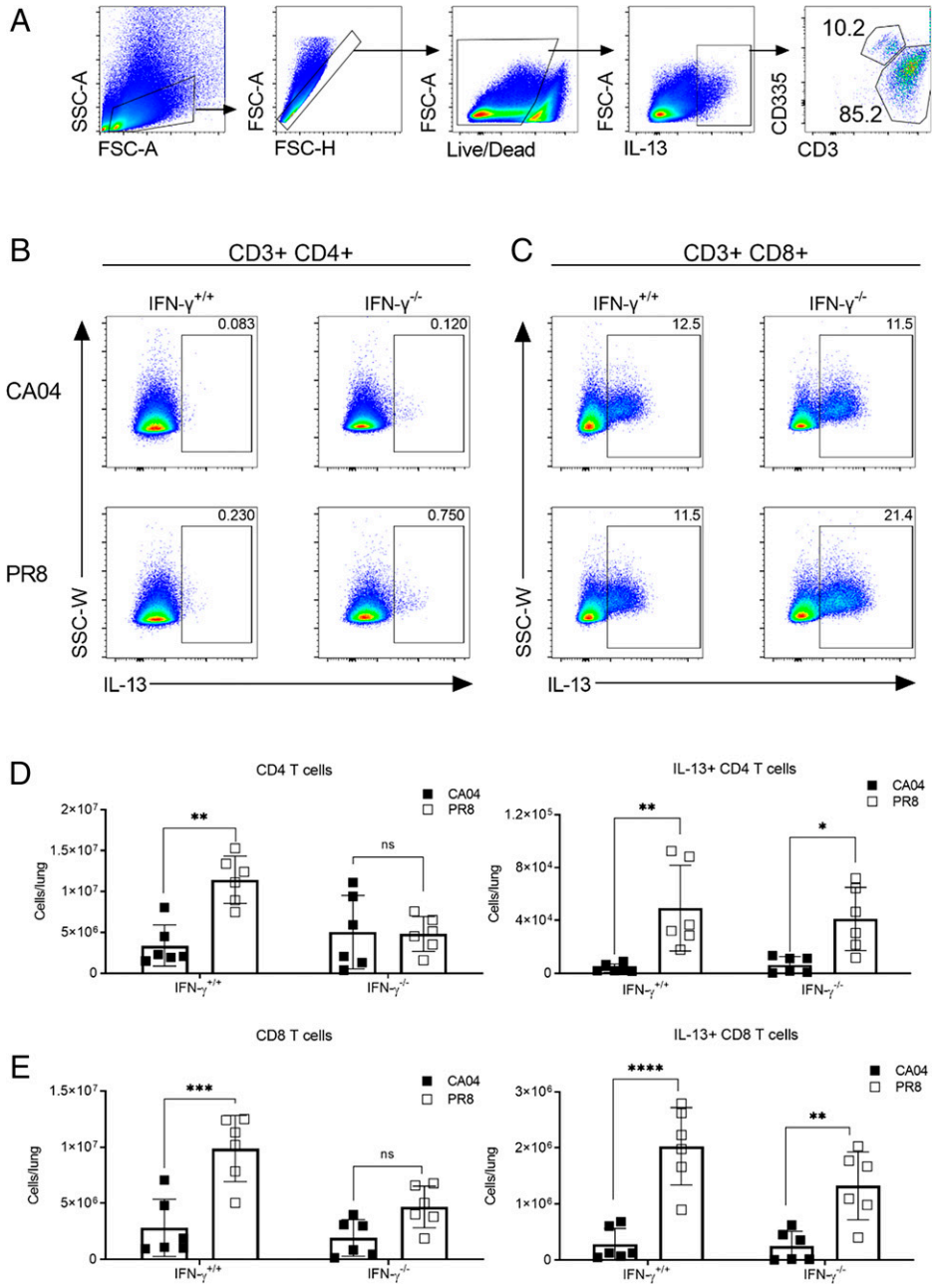

Fig. 7. IL-13 is produced by CD8 T cells and is not increased in IFN-$\gamma^{-/-}$ BALB/c mice following CA04 or PR8 viral infection. Lung cells were harvested 9 d after infection with 50 PFU/mouse and restimulated ex vivo with PMA (50 ng/mL) and ionomycin (500 ng/mL) in the presence of brefeldin A (10 μg/mL). (*A*) Flow cytometry confirmed the identity of most IL-13–positive cells as CD3 T cells. FSC, forward scatter; SSC, side scatter. Representative dot plots of $CD3^+CD4^+$ T cells (*B*) and $CD3^+CD8^+$ T cells (*C*) following CA04 or PR8 infection of BALB/c IFN-$\gamma^{+/+}$ and IFN-$\gamma^{-/-}$ mice. (*D*) Total CD4 and IL-13^+ CD4 T cells. (*E*) Total CD8 and IL-13^+ CD8 T cells in the lung tissues following CA04 or PR8 infection. The data are presented as means ± SD from 5 mice/group and are representative of two independent experiments. Statistical analyses were performed by two-way ANOVA. *$P < 0.05$; **$P < 0.01$; ***$P < 0.001$; and ****$P < 0.0001$.

was expressed by CD8 T cells. Growing evidence has shown that IFN-γ can limit ILC2 activity. After in vitro or in vivo stimulation with IL-33, ILC2 numbers and production of IL-5 was reduced by IFN-γ (37, 38). Similar effects were seen after infection of mice with *Nippostrongylus* (37, 39), after α-galactosylceramide–mediated in vivo activation of natural killer T (NKT) cells (40), and in a murine model of systemic lupus erythematous (41). In all cases, it was reported that IFN-γ inhibited production of IL-5 by ILC2s obtained from various organs. However, we have shown that during murine influenza ILC2 cytokine production can be differentially regulated by IFN-γ, with IL-5 predominantly expressed in response to CA04, but not PR8 virus, after IFN-γ neutralization. To our knowledge, this is the first description of differential regulation of ILC2 activity based upon the pathogen used for the challenge, results that have significant implications for viral pathogenesis. It has been reported that reduced levels of IFN-γ seen in influenza virus–infected $Rag2^{-/-}$ mice result in greater levels of IL-5, although effects on survival were not shown (42). IL-5 production usually promotes the recruitment of eosinophils and can play a role in tissue healing, particularly during viral infections (43–45). We also observed increased amphiregulin and IL-10 expression in the

absence of IFN-γ signaling. Although our previously published results indicate that heightened production of IL-5 in the absence of IFN-γ is most crucial to improved survival following CA04 virus infection (8), the precise role of amphiregulin and IL-10 in the CA04 virus challenge model remains to be fully clarified.

Influenza A virus (IAV) infection also stimulates production of type-I interferons to enhance innate immune protection against viral infection (46). Duerr et al. reported that type-I IFN signaling inhibits lung ILC2 activation during IAV infection as well as immunopathology (37). Moro et al. similarly reported that type-I (and type-II) interferons antagonize ILC2 activity in the context of parasitic infection (39). PB1-F2 protein is known to suppress IFN synthesis by reducing mitochondrial membrane potential (47). However, in our studies, we actually observed optimal, ILC2–protective activity in the absence of functional PB1-F2 (i.e., during CA04 viral infection, a condition that would be expected to cause increased type-I IFN expression). A full mechanistic understanding of PB1-F2–mediated inhibition of type-I IFN signaling and its impact on immunopathology clearly needs further investigation.

IL-13 increases mucus secretion, goblet cell hyperplasia and AHR, which are typically detrimental, although some investigators have reported beneficial effects in parasitic infections (48, 49). In influenza infection, IL-13 can compromise the epithelial barrier (50, 51) and predispose to a more severe form of disease (52), as also seen in our study. Furthermore, continuous production of IL-13 by macrophages following lung inflammation can result in chronic lung disease (53). We found that ILC2s stimulated by CA04 challenge expressed a robust IL-5 response but little IL-13, whereas following PR8 challenge, a significant IL-13 response was induced. Nevertheless, few ILC2-producing IL-13 could be detected in lung tissue by flow cytometry, prompting us to closely examine other cellular sources of IL-13. The major population of IL-13–secreting cells during PR8 infection was discovered to be CD8 T cells, regardless of the presence or absence of IFN-γ. Mice lacking IL-13 expression were rescued from PR8 lethality, indicating a pathologic role for IL-13 following influenza. The absence of IL-13 production during CA04 infection further indicated that functional PB1-F2 protein regulates CD8 T cells independently from IFN-γ. During SARS-CoV-2 lung infection, levels of IL-13 are increased in patients with severe COVID-19, and this causes immune dysregulation (54). In a mouse infection model, neutralization of IL-13 reduced disease severity and levels of pulmonary hyaluronan, highlighting the role of IL-13 in lung pathology (54). Also, IL-13^{+} T cells induced during *Chlamydia muridarum* infection have been associated with immunopathology (55). Taken together, various reports are in agreement with the levels of lethality we observed in response to PR8 virus infection. However, there is also evidence that IL-13 can increase resistance against other pathogens, such as *Leishmania major*, *Leishmania mexicana*, and *Listeria monocytogenes* (56).

By exploiting unique influenza virus reassortants, we were able to directly show that the observed differences in CA04 and PR8 infection outcome were due to the PB1-F2 viral gene. All viruses were fully capable of replicating in vitro in Madin–Darby canine kidney (MDCK) cells and in vivo in mice and, therefore, did not appear to have a defect in the RNA polymerase complex. Rather, CA04 virus–expressing PR8 PB1-F2 and PR8-expressing CA04 PB1-F2 induced an ILC2 phenotype and tissue pathogenicity similar to that of the PB1-F2 donor strains, demonstrating the role of PB1-F2 on ILC2 function. Our results indicate that activation of ILC2s can improve host survival following CA04 infection and that the PR8 PB1-F2 inhibits this ILC2-mediated protection. By histopathology analysis, the PR8 parent virus and the CA04 reassortant virus expressing PR8 PB1-F2 induced diffuse, necrotizing bronchitis and bronchiolitis, leading to the collapse of the alveoli and death of the mice. Similar observations of diffuse alveolar damage leading to the death of mice were reported by others with PR8 virus infection (57).

PB1-F2 is a proapoptotic protein that originates from an alternate open reading frame in the PB1 polymerase gene of most human and avian isolates (19, 27, 58). CA04 and PR8 viruses are both H1N1 strains, but the PB1-F2 of CA04 is truncated and nonfunctional, whereas the PR8 virus possesses a full-length and functional PB1-F2 (16–20). It has been reported that the PB1-F2 protein of the PR8 virus induces increased immunopathology and promotes apoptosis of immune cells (16, 19, 20), which agrees with our findings of increased ILC2 caspase expression following exposure to PR8 and improved tissue pathology and survival in IL-4$^{-/-}$ IL-13$^{-/-}$ mice after challenge with PR8 virus or reassortant CA04 virus containing PR8 PB1-F2, when compared to WT animals. Enhanced apoptosis and IL-13 expression during PR8 virus infection likely contribute to increased pathology compared to CA04 virus. It is known that PB1-F2 does not impact viral replication (16, 28), further indicating its major impact on host tissue integrity.

Our results show that the improved lung pathology and survival against challenge with CA04 virus and PR8 (CA04 PB1-F2) that was observed after neutralization of IFN-γ was dependent upon ILC2s. However, the presence or absence of ILC2s after PR8 or CA04 (PR8 PB1-F2) challenge had no apparent effect on lethality or tissue pathology. This is in agreement with our finding that PR8 infection induces a predominant subset of CD8 T cells that express IL-13. Conversely, IL-5 produced in CA04 virus–challenged animals is almost entirely derived from ILC2s. Thus, deficiency of ILC2s would be expected to abrogate production of IL-5, but not IL-13, which is consistent with our findings. Use of IFN-γR1$^{f/f}$ Rorα^{Cre} mice, which lack IFN-γ receptors specifically on ILC2s, confirmed that IFN-γ acts directly on ILC2s to decrease protection from lung pathology and overall survival in response to CA04, but not PR8, viral infection. IL-5 production in CA04-infected IFN-γR1$^{f/f}$ Rorα^{Cre} mice was greater than in WT littermate controls. Previous investigators, including ourselves, have reported the presence of the IFN-γR on ILC2s (8, 37, 39, 40). Thus, we conclude that the effect of IFN-γ during influenza is due to direct effects on ILC2s, rather than indirectly through intermediary cells.

In summary, we have shown that the PB1-F2 virulence factor of influenza virus acts in concert with host IFN-γ to regulate ILC2- and T cell–mediated recovery from viral disease. In the absence of both IFN-γ and influenza PB1-F2, ILC2s protect lung tissue from virus-induced damage and increase host resistance. This protection correlates with increased IL-5 production by ILC2s. However, in the presence of a functional PB1-F2, ILC2s produce less IL-5, leading to enhanced lethality. These findings demonstrate that both pathogen and host factors can regulate ILC2 activity to impact recovery from pulmonary viral infection.

Materials and Methods

Mouse Experiments. BALB/c IFN-γ$^{+/+}$ and IFN-γ$^{-/-}$ mice were purchased from Jackson Laboratories. ILC2-deficient Rora$^{f/f}$ IL7r^{cre} and IL-4$^{-/-}$IL-13$^{-/-}$ BALB/c were developed at the Medical Research Council, as described previously (34). Rorα^{cre} mice were kindly provided by Dr. Steven Zeigler, Benaroya Research Institute, Seattle, WA and bred with IFN-γR1$^{f/f}$ mice (Jackson Laboratories) at Albany Medical College. All mice were housed in a specific, pathogen-free environment. For virus infection, mice were anesthetized by isoflurane inhalation and inoculated i. n. with influenza virus. The animals were observed daily for weight loss, clinical signs of morbidity, and survival for a period of 20 d. Influenza virus replication was measured in BALF samples by plaque assay on MDCK cells. The Institutional Animal Care and Use Committee at Albany Medical College approved all experimental methods used in this study (protocol

Nos. 17–03006 and 20–04001). Details of all animal models used are described in *SI Appendix*, Table S1.

Generation of PB1-F2 Gene Reassortant Influenza Viruses. Viruses containing the PB1 gene from either PR8 or CA04 viruses were created as 1:7 reassortants using the well-established, eight-plasmid reverse genetic system, as described previously (59–61). Plasmids for PR8 and CA04 viruses were kindly provided by Richard J. Webby, St. Jude Children's Research Hospital, Memphis, TN. Viruses rescued from 293T: MDCK cell cocultures were propagated in 10-d-old embryonated chicken eggs for 72 h at 35 °C, and viral genome sequencing (Cambridge Technologies, Worthington, MN) was used to confirm the anticipated genotype. The PR8 (CA04 PB1-F2, OM488259-OM488266) and CA04 (PR8 PB1-F2, OM486956-OM486963) viruses produced essentially equivalent numbers of PFU after growth in MDCK cells. In addition, the WT parent viruses present at Albany Medical College for over 10 y matched the reassortment viruses made at University of South Dakota for viral PFU.

Details of all WT and reassortant viruses are mentioned in *SI Appendix*, Table S2.

Flow Cytometry Analysis. Lung tissue was digested in 3 mL digestion buffer composed of PBS, 2 mg/mL Liberase TL (Roche Diagnostics GmbH), and 10 mg/mL DNase I (Roche Diagnostics GmbH) at 37 °C for 0.5 h and then filtered through a 40-μm filter with Roswell Park Memorial Institute medium 1640 containing 10% fetal bovine serum. Red blood cell lysis was performed using ammonium-chloride-potassium buffer. Single-cell suspensions from lungs and BAL were incubated with FcγRII/III block (2.4G2 mAb) for 15 min and then stained with anti-mouse mAbs followed by fixable viability dye to differentiate live and dead cells. Antibodies used for flow cytometry analysis are listed in the Key Resources table. For intracellular cytokine staining of T cells and ILC2s, cells were stimulated ex vivo for 3 to 4 h with 50 ng/mL PMA, 500 ng/mL ionomycin, and 10 μg/mL brefeldin A at 37 °C. Cells were then stained for surface markers, followed by fixation in 2% paraformaldehyde, permeabilization in BD perm/wash buffer, and incubation with intracellular cytokine mAbs. The stained cells were analyzed on a BD fluorescence-activated single cell sorter (FACS) Canto or LSR II using FACSDiva. Flow cytometry data were analyzed using FlowJo software (BD). ILC2s were designated as cells that were positive for CD90.2 (Thy1.2), KLRG1, and CD127 (IL-7R) but negative for the lineage markers for T cells (CD3, CD5, and TCRβ), B cells (CD45R), NK cells (CD335), and myeloid cells (TER-119, CD11b, and Gr-1). IL-13+ T cells were identified as IL-13+ and CD3+ and further characterized based on expression of CD4 and CD8. Antibodies and all essential chemical/reagent used for this study are mentioned in *SI Appendix*, Tables S3 and S4.

Measurement of Cytokines/Chemokines. Lungs were washed three times with PBS to obtain BAL, and the cell-free supernatants were analyzed for IL-2, IL-4, IL-5, IL-9, IL-10, IL-12, IL-13, IL-17, amphiregulin, TNF-α, GM-CSF, and IFN-γ by enzyme linked immunosorbent assay using methods recommended by the manufacturers (BD Biosciences, eBioscience, and R&D Systems). Levels of albumin in BALF were determined with the bacillus Calmette–Guérin albumin assay kit (Sigma-Aldrich). Total protein concentrations in BALF were analyzed using a Micro bicinchoninic acid protein assay kit (Thermo Fisher Scientific). Nitrite levels were quantified using a colorimetric Griess reagent kit (Life Technologies). The critical commercial kits used here are mentioned in *SI Appendix*, Table S5.

Caspase 3/7 Apoptosis Analysis. To assess apoptosis induced by PR8 versus CA04 virus, BALB/c mice were infected with 2,000 PFU of CA04 and PR8 viruses. Control mice received PBS. Around 5 d later, the mice were euthanized, and BAL was collected in α-minimum essential medium (MEM) containing 1 ng/mL rIL-33 (R&D Systems) and 10 ng/mL IL-2 (R&D Systems). In addition, a murine ILC2 cell line (kindly provided by Dr. Qi Yang, Albany Medical College, Albany, NY) was incubated for 5 d with BALF from the above virus-infected mice. All cells were then assessed for apoptosis using the Caspase-Glo 3/7 (Table 5), as per the manufacturer's protocol (Promega). Caspase activity was reported as a mean relative light units.

Histopathology Analysis of Lung Tissue. For histopathology analysis, lung tissues were fixed in 10% formalin and 5-μm tissue sections were stained with hematoxylin and eosin. A histopathology scoring system was used based upon known pathological features of influenza virus infection (57, 62, 63). The scoring included the presence and extent of inflammatory infiltrates, edema, hyperemia and congestion, focal necrosis of alveolar epithelium, and necrotizing bronchitis and bronchiolitis. For evaluation of mucus production, periodic acid–Schiff Alcian blue staining was performed. A total of 10 fields from both left and right lung sections were examined under a microscope in a double-blinded manner by a veterinary pathologist to determine histopathology scores, as described by others (64). The scoring criteria were the following: 0 for no changes, 1 for mild changes, 2 for moderate changes, 3 for marked changes, and 4 for severe changes. Images were captured with an Olympus BX41 microscope (Olympus) under 20× magnification. Images were acquired using CellSense software.

Measurement of Lung Edema. Lung edema was measured as previously described (65). After euthanasia, lungs were collected, blotted dry, and wet weight was determined using an AX105 Delta Range analytical balance (Mettler Toledo). The lungs were then incubated at 60 °C for 72 h and reweighed as dry weight. The ratio of wet lung/dry lung weight was used to determine the amount of tissue edema.

Statistical Analysis. Data are expressed as means ± SD. Survival curves were evaluated by log-rank Mantel–Cox test, and weight loss data were analyzed by using a two-tailed Mann–Whitney *U* test. Statistical significance between groups was determined using a two-tailed Student's *t* test (to compare two samples), ANOVA followed by Tukey's/Bonferroni's multiple comparisons test (to compare multiple samples), or a two-tailed Mann–Whitney *U* test (nonparametric test). All statistical calculations were performed in GraphPad Prism (GraphPad Software, Inc). For all analyses, a P value <0.05 was considered significant.

Data Availability. The gene sequences of the reassortant viruses have been deposited at GenBank (OM488259, OM488260, OM488261, OM488262, OM488263, OM488264, OM488265, and OM488266 for PR8(CA04 PB1-F2) and OM486956, OM486957, OM486958, OM486959, OM486960, OM486961, OM486962, and OM486963 for CA04(PR8 PB1-F2). All other data needed to draw the conclusions are available within the manuscript. All study data are included in the article and/or *SI Appendix*.

ACKNOWLEDGMENTS. We thank Dr. Steven F. Zeigler for kindly providing the Rorα^{Cre} mice, Dr. Qi Yang for providing the murine ILC2 cell line, and Heather Hajovsky for her technical expertise in creating the reassortant viruses by reverse genetics. We also thank the Department of Immunology and Microbial Disease Immunology Core Laboratory for assistance in histology analyses. This work was supported by NIH grants RO1 HL140496 to D.W.M. and P20 GM103443 to V.C.H.

1. J. Sun, T. J. Braciale, Role of T cell immunity in recovery from influenza virus infection. *Curr. Opin. Virol.* **3**, 425–429 (2013).
2. E. Vivier *et al.*, Innate lymphoid cells: 10 years on. *Cell* **174**, 1054–1066 (2018).
3. A. Srikiatkhachorn *et al.*, Interference with intraepithelial TNF-α signaling inhibits CD8(+) T-cell-mediated lung injury in influenza infection. *Viral Immunol.* **23**, 639–645 (2010).
4. T. Veiga-Parga, S. Sehrawat, B. T. Rouse, Role of regulatory T cells during virus infection. *Immunol. Rev.* **255**, 182–196 (2013).
5. N. L. La Gruta, S. J. Turner, T cell mediated immunity to influenza: Mechanisms of viral control. *Trends Immunol.* **35**, 396–402 (2014).
6. L. A. Monticelli *et al.*, Innate lymphoid cells promote lung-tissue homeostasis after infection with influenza virus. *Nat. Immunol.* **12**, 1045–1054 (2011).
7. Y.-J. Chang *et al.*, Innate lymphoid cells mediate influenza-induced airway hyperreactivity independently of adaptive immunity. *Nat. Immunol.* **12**, 631–638 (2011).
8. D. Califano *et al.*, IFN-γ increases susceptibility to influenza A infection through suppression of group II innate lymphoid cells. *Mucosal Immunol.* **11**, 209–219 (2018).
9. N. Rodriguez-Rodriguez, M. Gogoi, A. N. J. McKenzie, Group 2 innate lymphoid cells: Team players in regulating asthma. *Annu. Rev. Immunol.* **39**, 167–198 (2021).
10. K. Moro *et al.*, Innate production of T(H)2 cytokines by adipose tissue-associated c-Kit(+)Sca-1(+) lymphoid cells. *Nature* **463**, 540–544 (2010).
11. D. R. Neill *et al.*, Nuocytes represent a new innate effector leukocyte that mediates type-2 immunity. *Nature* **464**, 1367–1370 (2010).
12. A. E. Price *et al.*, Systemically dispersed innate IL-13-expressing cells in type 2 immunity. *Proc. Natl. Acad. Sci. U.S.A.* **107**, 11489–11494 (2010).
13. S. A. Saenz *et al.*, IL25 elicits a multipotent progenitor cell population that promotes T(H)2 cytokine responses. *Nature* **464**, 1362–1366 (2010).
14. J. L. Barlow *et al.*, Innate IL-13-producing nuocytes arise during allergic lung inflammation and contribute to airways hyperreactivity. *J. Allergy Clin. Immunol.* **129**, 191–198.e1-4 (2012).
15. K. R. Bartemes *et al.*, IL-33-responsive lineage- CD25+ CD44(hi) lymphoid cells mediate innate type 2 immunity and allergic inflammation in the lungs. *J. Immunol.* **188**, 1503–1513 (2012).
16. D. Zamarin, M. B. Ortigoza, P. Palese, Influenza A virus PB1-F2 protein contributes to viral pathogenesis in mice. *J. Virol.* **80**, 7976–7983 (2006).
17. T. T. Wang, P. Palese, Unraveling the mystery of swine influenza virus. *Cell* **137**, 983–985 (2009).

18. L. Pena *et al.*, Restored PB1-F2 in the 2009 pandemic H1N1 influenza virus has minimal effects in swine. *J. Virol.* **86**, 5523–5532 (2012).
19. W. Chen *et al.*, A novel influenza A virus mitochondrial protein that induces cell death. *Nat. Med.* **7**, 1306–1312 (2001).
20. G. Neumann, T. Noda, Y. Kawaoka, Emergence and pandemic potential of swine-origin H1N1 influenza virus. *Nature* **459**, 931–939 (2009).
21. M. B. Graham *et al.*, Response to influenza infection in mice with a targeted disruption in the interferon gamma gene. *J. Exp. Med.* **178**, 1725–1732 (1993).
22. S. R. Sarawar, M. Sangster, R. L. Coffman, P. C. Doherty, Administration of anti-IFN-gamma antibody to beta 2-microglobulin-deficient mice delays influenza virus clearance but does not switch the response to a T helper cell 2 phenotype. *J. Immunol.* **153**, 1246–1253 (1994).
23. H. B. Suliman, L. K. Ryan, L. Bishop, R. J. Folz, Prevention of influenza-induced lung injury in mice overexpressing extracellular superoxide dismutase. *Am. J. Physiol. Lung Cell. Mol. Physiol.* **280**, L69–L78 (2001).
24. S. Shalini, L. Dorstyn, S. Dawar, S. Kumar, Old, new and emerging functions of caspases. *Cell Death Differ.* **22**, 526–539 (2015).
25. N. Van Opdenbosch, M. Lamkanfi, Caspases in cell death, inflammation, and disease. *Immunity* **50**, 1352–1364 (2019).
26. G. M. Conenello, D. Zamarin, L. A. Perrone, T. Tumpey, P. Palese, A single mutation in the PB1-F2 of H5N1 (HK/97) and 1918 influenza A viruses contributes to increased virulence. *PLoS Pathog.* **3**, 1414–1421 (2007).
27. R. Zell *et al.*, Prevalence of PB1-F2 of influenza A viruses. *J. Gen. Virol.* **88**, 536–546 (2007).
28. J. L. McAuley, K. Zhang, J. A. McCullers, The effects of influenza A virus PB1-F2 protein on polymerase activity are strain specific and do not impact pathogenesis. *J. Virol.* **84**, 558–564 (2010).
29. J. L. McAuley *et al.*, Expression of the 1918 influenza A virus PB1-F2 enhances the pathogenesis of viral and secondary bacterial pneumonia. *Cell Host Microbe* **2**, 240–249 (2007).
30. R. Le Goffic *et al.*, Transcriptomic analysis of host immune and cell death responses associated with the influenza A virus PB1-F2 protein. *PLoS Pathog.* **7**, e1002202 (2011).
31. I. V. Alymova *et al.*, A novel cytotoxic sequence contributes to influenza A viral protein PB1-F2 pathogenicity and predisposition to secondary bacterial infection. *J. Virol.* **88**, 503–515 (2014).
32. D. Califano, Y. Furuya, D. W. Metzger, Effects of influenza on alveolar macrophage viability are dependent on mouse genetic strain. *J. Immunol.* **201**, 134–144 (2018).
33. H. E. Ghoneim, P. G. Thomas, J. A. McCullers, Depletion of alveolar macrophages during influenza infection facilitates bacterial superinfections. *J. Immunol.* **191**, 1250–1259 (2013).
34. C. J. Oliphant *et al.*, MHCII-mediated dialog between group 2 innate lymphoid cells and CD4(+) T cells potentiates type 2 immunity and promotes parasitic helminth expulsion. *Immunity* **41**, 283–295 (2014).
35. S. L. LaPorte *et al.*, Molecular and structural basis of cytokine receptor pleiotropy in the interleukin-4/13 system. *Cell* **132**, 259–272 (2008).
36. G. Marone *et al.*, The intriguing role of interleukin 13 in the pathophysiology of asthma. *Front. Pharmacol.* **10**, 1387 (2019).
37. C. U. Duerr *et al.*, Type I interferon restricts type 2 immunopathology through the regulation of group 2 innate lymphoid cells. *Nat. Immunol.* **17**, 65–75 (2016).
38. A. B. Molofsky *et al.*, Interleukin-33 and interferon-gamma counter-regulate group 2 innate lymphoid cell activation during immune perturbation. *Immunity* **43**, 161–174 (2015).
39. K. Moro *et al.*, Interferon and IL-27 antagonize the function of group 2 innate lymphoid cells and type 2 innate immune responses. *Nat. Immunol.* **17**, 76–86 (2016).
40. F. Kudo *et al.*, Interferon-γ constrains cytokine production of group 2 innate lymphoid cells. *Immunology* **147**, 21–29 (2016).
41. M. Düster *et al.*, T cell-derived IFN-γ downregulates protective group 2 innate lymphoid cells in murine lupus erythematosus. *Eur. J. Immunol.* **48**, 1364–1375 (2018).
42. S. A. Gorski, Y. S. Hahn, T. J. Braciale, Group 2 innate lymphoid cell production of IL-5 is regulated by NKT cells during influenza virus infection. *PLoS Pathog.* **9**, e1003615 (2013).
43. A. E. Samarasinghe *et al.*, Eosinophils promote antiviral immunity in mice infected with influenza A virus. *J. Immunol.* **198**, 3214–3226 (2017).
44. S. Phipps *et al.*, Eosinophils contribute to innate antiviral immunity and promote clearance of respiratory syncytial virus. *Blood* **110**, 1578–1586 (2007).
45. D. J. Adamko, B. L. Yost, G. J. Gleich, A. D. Fryer, D. B. Jacoby, Ovalbumin sensitization changes the inflammatory response to subsequent parainfluenza infection. Eosinophils mediate airway hyperresponsiveness, m(2) muscarinic receptor dysfunction, and antiviral effects. *J. Exp. Med.* **190**, 1465–1478 (1999).
46. J.-K. Yoo, T. S. Kim, M. M. Hufford, T. J. Braciale, Viral infection of the lung: Host response and sequelae. *J. Allergy Clin. Immunol.* **132**, 1263–1276 (2013).
47. Z. T. Varga, A. Grant, B. Manicassamy, P. Palese, Influenza virus protein PB1-F2 inhibits the induction of type I interferon by binding to MAVS and decreasing mitochondrial membrane potential. *J. Virol.* **86**, 8359–8366 (2012).
48. M. Sköld, S. M. Behar, Role of CD1d-restricted NKT cells in microbial immunity. *Infect. Immun.* **71**, 5447–5455 (2003).
49. S. Gordon, F. O. Martinez, Alternative activation of macrophages: Mechanism and functions. *Immunity* **32**, 593–604 (2010).
50. Z.-Q. Huang *et al.*, Interleukin-13 alters tight junction proteins expression thereby compromising barrier function and dampens rhinovirus induced immune responses in nasal epithelium. *Front. Cell Dev. Biol.* **8**, 572749 (2020).
51. B. Saatian *et al.*, Interleukin-4 and interleukin-13 cause barrier dysfunction in human airway epithelial cells. *Tissue Barriers* **1**, e24333 (2013).
52. M. R. Starkey *et al.*, Interleukin-13 predisposes to more severe influenza infection in mice and human epithelial cells by suppressing interferon responses and activating the microRNA-21/PI3K signaling pathway. *Am. J. Respir. Crit. Care Med.* **195**, A4926 (2017).
53. E. Y. Kim *et al.*, Persistent activation of an innate immune response translates respiratory viral infection into chronic lung disease. *Nat. Med.* **14**, 633–640 (2008).
54. A. N. Donlan *et al.*, IL-13 is a driver of COVID-19 severity. *JCI Insight* **6**, e150107 (2021).
55. R. M. Johnson, M. S. Kerr, J. E. Slaven, An atypical CD8 T-cell response to *Chlamydia muridarum* genital tract infections includes T cells that produce interleukin-13. *Immunology* **142**, 248–257 (2014).
56. T. A. Wynn, IL-13 effector functions. *Annu. Rev. Immunol.* **21**, 425–456 (2003).
57. M. Fukushi *et al.*, Serial histopathological examination of the lungs of mice infected with influenza A virus PR8 strain. *PLoS One* **6**, e21207 (2011).
58. M. Henkel *et al.*, The proapoptotic influenza A virus protein PB1-F2 forms a nonselective ion channel. *PLoS One* **5**, e11112 (2010).
59. V. C. Huber, L. H. Kleimeyer, J. A. McCullers, Live, attenuated influenza virus (LAIV) vehicles are strong inducers of immunity toward influenza B virus. *Vaccine* **26**, 5381–5388 (2008).
60. K. McCormick *et al.*, Construction and immunogenicity evaluation of recombinant influenza A viruses containing chimeric hemagglutinin genes derived from genetically divergent influenza A H1N1 subtype viruses. *PLoS One* **10**, e0127649 (2015).
61. Z. Li *et al.*, A chimeric influenza hemagglutinin delivered by parainfluenza virus 5 vector induces broadly protective immunity against genetically divergent influenza a H1 viruses in swine. *Vet. Microbiol.* **250**, 108859 (2020).
62. K. N. Gibson-Corley, A. K. Olivier, D. K. Meyerholz, Principles for valid histopathologic scoring in research. *Vet. Pathol.* **50**, 1007–1015 (2013).
63. J. K. Taubenberger, D. M. Morens, The pathology of influenza virus infections. *Annu. Rev. Pathol.* **3**, 499–522 (2008).
64. J. P. Buchweitz, P. W. F. Karmaus, J. R. Harkema, K. J. Williams, N. E. Kaminski, Modulation of airway responses to influenza A/PR/8/34 by Delta9-tetrahydrocannabinol in C57BL/6 mice. *J. Pharmacol. Exp. Ther.* **323**, 675–683 (2007).
65. G. S. Whitehead, L. H. Burch, K. G. Berman, C. A. Piantadosi, D. A. Schwartz, Genetic basis of murine responses to hyperoxia-induced lung injury. *Immunogenetics* **58**, 793–804 (2006).